



HAL
open science

Nanoindentation of Mesenchymal Stem Cells using Atomic Force Microscopy: Effect of Adhesive Cell-Substrate Structures

Elisa Migliorini, Elisabetta Ada Cavalcanti-Adam, Antonio Emmanuele Uva, Michele Fiorentino, Michele Gattullo, Vito Modesto Manghisi, Lorenzo Vaiani, Antonio Boccaccio

► **To cite this version:**

Elisa Migliorini, Elisabetta Ada Cavalcanti-Adam, Antonio Emmanuele Uva, Michele Fiorentino, Michele Gattullo, et al.. Nanoindentation of Mesenchymal Stem Cells using Atomic Force Microscopy: Effect of Adhesive Cell-Substrate Structures. *Nanotechnology*, 2021, 32 (21), pp.215706. 10.1088/1361-6528/abe748 . hal-03152740

HAL Id: hal-03152740

<https://hal.science/hal-03152740>

Submitted on 25 Feb 2021

HAL is a multi-disciplinary open access archive for the deposit and dissemination of scientific research documents, whether they are published or not. The documents may come from teaching and research institutions in France or abroad, or from public or private research centers.

L'archive ouverte pluridisciplinaire **HAL**, est destinée au dépôt et à la diffusion de documents scientifiques de niveau recherche, publiés ou non, émanant des établissements d'enseignement et de recherche français ou étrangers, des laboratoires publics ou privés.

ACCEPTED MANUSCRIPT

Nanoindentation of Mesenchymal Stem Cells using Atomic Force Microscopy: Effect of Adhesive Cell-Substrate Structures

To cite this article before publication: Elisa Migliorini *et al* 2021 *Nanotechnology* in press <https://doi.org/10.1088/1361-6528/abe748>

Manuscript version: Accepted Manuscript

Accepted Manuscript is “the version of the article accepted for publication including all changes made as a result of the peer review process, and which may also include the addition to the article by IOP Publishing of a header, an article ID, a cover sheet and/or an ‘Accepted Manuscript’ watermark, but excluding any other editing, typesetting or other changes made by IOP Publishing and/or its licensors”

This Accepted Manuscript is © 2021 IOP Publishing Ltd.

During the embargo period (the 12 month period from the publication of the Version of Record of this article), the Accepted Manuscript is fully protected by copyright and cannot be reused or reposted elsewhere.

As the Version of Record of this article is going to be / has been published on a subscription basis, this Accepted Manuscript is available for reuse under a CC BY-NC-ND 3.0 licence after the 12 month embargo period.

After the embargo period, everyone is permitted to use copy and redistribute this article for non-commercial purposes only, provided that they adhere to all the terms of the licence <https://creativecommons.org/licenses/by-nc-nd/3.0>

Although reasonable endeavours have been taken to obtain all necessary permissions from third parties to include their copyrighted content within this article, their full citation and copyright line may not be present in this Accepted Manuscript version. Before using any content from this article, please refer to the Version of Record on IOPscience once published for full citation and copyright details, as permissions will likely be required. All third party content is fully copyright protected, unless specifically stated otherwise in the figure caption in the Version of Record.

View the [article online](#) for updates and enhancements.

Nanoindentation of Mesenchymal Stem Cells using Atomic Force Microscopy: Effect of Adhesive Cell-Substrate Structures

Elisa Migliorini¹, Elisabetta Ada Cavalcanti-Adam^{2,3}, Antonio E. Uva⁴, Michele Fiorentino⁴,
Michele Gattullo⁴, Vito Modesto Manghisi⁴, Lorenzo Vaiani⁴, Antonio Boccaccio^{4*}

¹CNRS UMR 5628 (LMGP), Grenoble 38016, France

²Max Planck Institute for Medical Research, D-69120 Heidelberg, Germany

³Heidelberg University, D-69120 Heidelberg, Germany

⁴Dipartimento di Meccanica, Matematica e Management, Politecnico di Bari, Bari, Italy

*Corresponding author:

Antonio Boccaccio, Associate Professor

Dipartimento di Meccanica, Matematica e Management (DMMM)

Politecnico di Bari

Campus "Ernesto Quagliariello"

Via Edoardo Orabona, 4

I-70125 Bari

Italy

Tel. +39 080 5963393

Abstract

The procedure commonly adopted to characterize cell materials using atomic force microscopy neglects the stress state induced in the cell by the adhesion structures that anchor it to the substrate. In several studies, the cell is considered as made from a single material and no specific information is provided regarding the mechanical properties of subcellular components. Here we present an optimization algorithm to determine separately the material properties of subcellular components of mesenchymal stem cells subjected to nanoindentation measurements. We assess how these properties change if the adhesion structures at the cell-substrate interface are considered or not in the algorithm. In particular, among the adhesion structures, the focal adhesions and the stress fibers were simulated. We found that neglecting the adhesion structures leads to underestimate the cell mechanical properties thus making errors up to 15%. This result leads us to conclude that the action of adhesion structures should be taken into account in nanoindentation measurements especially for cells that include a large number of adhesions to the substrate.

Keywords: stress fibers, focal adhesion, finite element method, cytoskeleton, cell cortex, cell mechanics

1. Introduction

Atomic Force Microscopy (AFM) is a commonly utilized technique to characterize the mechanical behavior of cell materials [1]. The effect of cell sample size [2] as well as of cell spreading and contractility [3] on stiffness measurements using AFM was investigated. The issues related to the AFM tip shape and to how this affects the mechanical characterization of cell materials were also addressed in previous studies [4,5]. AFM has been so far successfully applied to investigate different cell types, such as endothelial cells [6], leukocytes [7], hair cells [8], skeletal muscle cells [9], cardiocytes [10], erythrocytes [11,12], chondrocytes [13], oocytes [14–16], colorectal [17–19] and oral [20] cancer cell lines. Among the other cell lines, also stem cells have been characterized by AFM [21–24]. The knowledge of stem cells mechanical properties is of fundamental importance to investigate their mechanobiological behavior. Most of the computational mechano-regulation models available in the literature [25–29] that define the relationships between the biophysical stimulus acting on stem cells and how they differentiate into different phenotypes, rely on the accurate knowledge of stem cells mechanics and their structural response to mechanical stimuli.

In almost all the studies available in the literature, the determination of the cell mechanical properties via AFM is carried out by implementing the Hertz contact theory [30]. This theory, based on specific hypotheses, establishes an explicit relationship between the force F exerted by the indenter, the indentation δ (i.e. the displacement) imposed to the indenter, and the cell Young's modulus E_H . Nowadays, most of the AFM devices available on the market are equipped with software tools that implement this theory. The hypotheses of the Hertz contact theory are very strict: (i) the strains induced in the indented material are

1
2
3 infinitesimal, (ii) the dimension of the contact area is small; (iii) the bodies put in contact
4
5 behave as linearly elastic materials; (iv) the indented material behaves as an infinite elastic
6
7 half-space. In general, not all the above-mentioned hypotheses are satisfied in the cell
8
9 nanoindentation process. Cells can experience very large deformations and typically behave
10
11 as hyperelastic (and not simply elastic) materials [31]. Another important limitation of the
12
13 approach based on the Hertz contact theory is that it neglects the pre-stress/strain state acting
14
15 on the cell – which is typically attached to a substrate – before the nanoindentation process
16
17 takes place. It is commonly known that a cell attached to a substrate experiences a
18
19 stress/strain state that is, in general, different with respect to that of the same cell free to move
20
21 [32]. Adhesive structures, i.e. specialized protein complexes, anchor the cell to the substrate.
22
23
24 Among the adhesive structures, certainly, focal adhesions and stress fibers play a crucial role
25
26 in establishing and maintaining cell-substrate interactions. Focal adhesions are micron-sized
27
28 protein assemblies mediated by integrins, which are transmembrane receptors that establish
29
30 the adhesion and the mechanical coupling between the ventral side of the cell and the
31
32 extracellular matrix (ECM) [33–35]. On the cytoplasmic side of these structures, the terminal
33
34 ends of microfilament bundles known as stress fibers, are anchored [36]. Stress fibers are
35
36 contractile bundles of actomyosin that mechanically interact not only with focal adhesions,
37
38 – through focal adhesions the stress fibers are anchored to the integrins, and therefore to the
39
40 substrate – but also with additional cellular structures, including neighboring stress fibers and
41
42 the cell cortex [37]. Due to the interaction between the focal adhesions and the stress fibers
43
44 a complex stress/strain state acts on the cell which will certainly affect the nanoindentation
45
46 and hence, the mechanical characterization process [32]. Another limitation of the Hertz
47
48 contact theory is that the cell is hypothesized to be made from a single material, which means,
49
50
51
52
53
54
55
56 in other words, that the Hertz theory cannot characterize distinctly the material properties of
57
58
59
60

1
2
3 different subcellular components such as the cell cortex, the cytoskeleton, and so on.
4
5 Practically, the Hertz theory allows determining just an “average” value of the mechanical
6
7 properties of the entire cell considered as a homogeneous entity made from a single type of
8
9 material. However, neglecting the subcellular components leads to make incorrect
10
11 evaluations of the cell mechanical properties. For instance, as demonstrated by Vargas-Pinto
12
13 et al. [38], implementing the Hertz theory and neglecting the presence of the cell cortex leads
14
15 to obtain different values of mechanical properties depending on the specific shape of the
16
17 AFM tip utilized in the nanoindentation measurements.
18
19

20
21 In this study, we developed a hybrid approach for the mechanical characterization of
22
23 mesenchymal stem cells (MSCs). MSCs were first nanoindented with AFM, then the
24
25 obtained force-indentation curves were incorporated within an optimization algorithm that
26
27 iteratively compares them with those predicted via a finite element model. The proposed
28
29 hybrid approach allows:
30
31

- 32
33 (i) taking into account the pre-stress/strain state acting on the cell due to the action of
34
35 adhesive structures at the cell/substrate interface;
36
37 (ii) determining separately the values of the mechanical properties of sub-cellular
38
39 components such as the cell cortex and the cytoskeleton;
40
41 (iii) overcoming the limitations of the Hertz contact theory knowing that the related
42
43 hypotheses are not fully satisfied in the nanoindentation process. The model
44
45 utilized in this study takes into account the hyperelastic constitutive behavior and
46
47 the regimen of large deformations.
48
49

50
51 We found that neglecting the effect of adhesive structures leads to underestimate the
52
53 cell mechanical properties.
54
55

2. Materials and methods

2.1. Cell culture

Mesenchymal stem cells from human primary material (hMSCs), donated by the Professor Ho group from the Department of Medicine V, Heidelberg University, were used for AFM indentation studies. hMSCs were isolated and cultured as described in previous studies [39,40]. Briefly, bone marrow from healthy donors for allogeneic transplantation was taken after written consent using guidelines approved by the Ethic Committee on the use of Human subjects at the Heidelberg University. After seeding of the mononuclear cell fraction evolving colonies were separated and hMSC further expanded in plastic culture flasks.

2.2. Sample preparation

hMSCs were detached with Accutase (Sigma Aldrich) from the flask and plated on glass cover slips (24×24 mm²; Menzel Gläser, Braunschweig, Germany), previously coated with 1 mg/mL of Fibronectin (Sigma) diluted in PBS. 20 nM of bone morphogenetic protein 2 (purchased from R&D Systems Inc. Minneapolis, MN, USA) has been added to the media to induce osteogenic differentiation of hMSCs. This differentiation media has been replaced once during the first week and just before the experiment.

2.3. Nanoindentation measurements

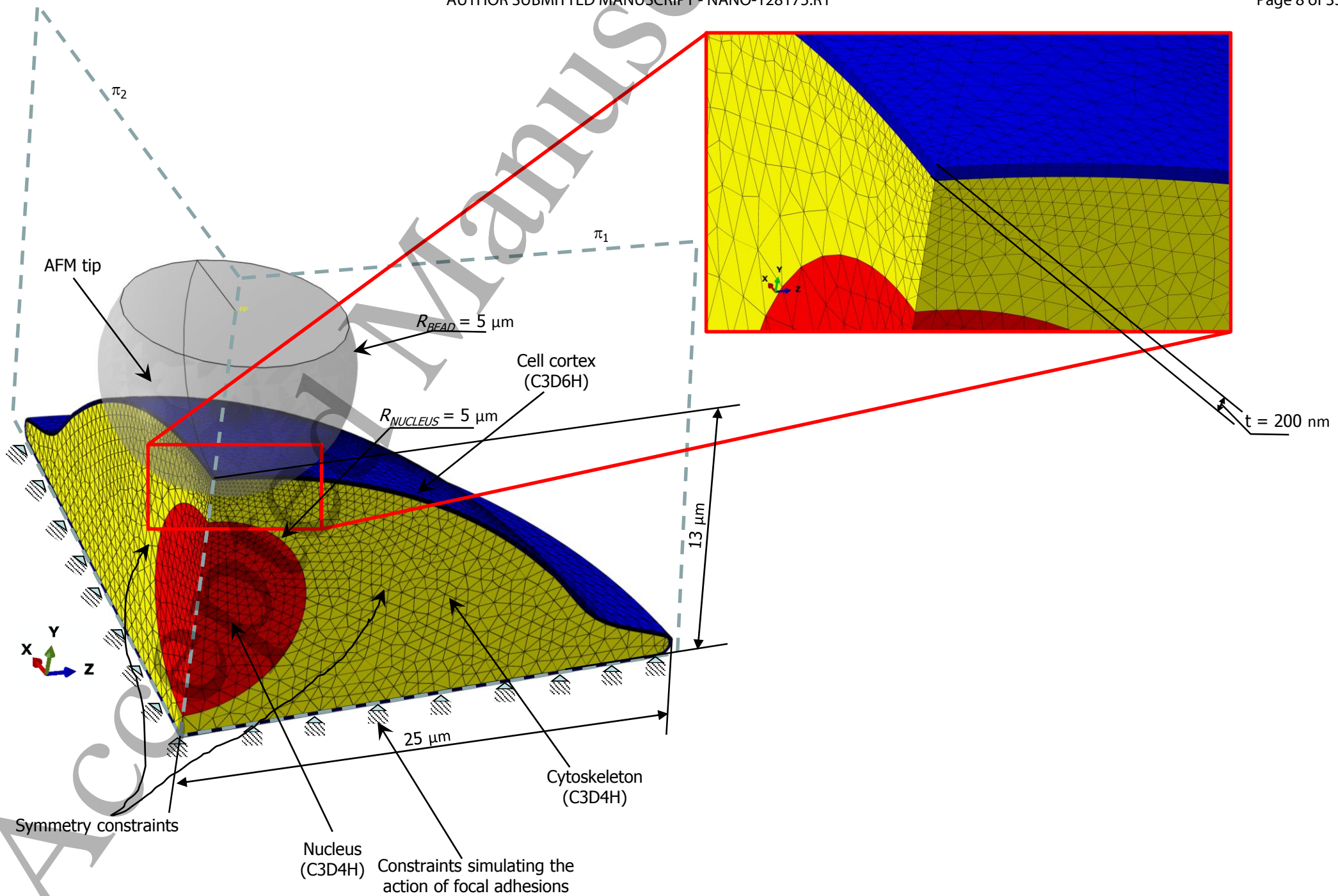
1
2
3 The cell indentation experiment was realized with an AFM (Nano Wizard, JPK Instruments,
4 Berlin) combined with an inverted optical microscope (Zeiss Axiovert 200) as previously
5 reported in Vaiani et al. [41]. Cantilevers (CP-qp-SCONTBSG from sQUBE) with a colloidal
6 probe (radius $R = 5 \mu\text{m}$) made of borosilicate glass were used.
7
8
9

10
11
12 The stiffness of hMSCs one week after osteogenic media replacement was tested. We
13 set the AFM to have a maximal indentation value no larger than 200 nm. In this range, the
14 forces applied by the cantilever to the sample were always $<5 \text{ nN}$. For the calculation of the
15 cellular mechanical properties we averaged five curves taken at the highest point of the cell
16 and we repeated the measurements on ten different hMSCs. The “average” curve obtained
17 for each of the ten cells, was hence used in the optimization algorithm described below.
18
19
20
21
22
23
24
25

26 27 28 *2.4. Finite element model of the nanoindented mesenchymal stem cell*

29
30
31

32 Utilizing the CAD tools available in ABAQUS 6.12[®], the finite element model simulating
33 the nanoindentation process of stem cells was built. The dimensions hypothesized for the
34 model (Figure 1) are the average dimensions typically measured for cells of mesenchymal
35 origin [42]. The subcellular components included in the model were: the nucleus (highlighted
36 in red, Figure 1), the cytoskeleton (highlighted in yellow, Figure 1), and the cell cortex
37 (highlighted in blue, Figure 1). Nucleus and cytoskeleton were discretized with 4-node linear
38 tetrahedrons, hybrid, with linear pressure elements C3D4H available in Abaqus, whereas the
39 cell cortex was modeled with 6-node linear triangular prisms, hybrid, with constant pressure
40 elements C3D6H (Figure 1). According to a previous studies[19,41], the cell cortex thickness
41 was set equal to $t = 200 \text{ nm}$ (Figure 1). To reduce the computational cost of the analyses, 1/4
42 of the entire model, delimited by the symmetry planes π_1 and π_2 , was considered and
43
44
45
46
47
48
49
50
51
52
53
54
55
56
57
58
59
60



45 **Figure 1.** One-quarter finite element model of the nanoindented mesenchymal stem cell utilized in the study and detailed view of the cell region coming in contact with the AFM tip.

submitted to finite element analyses (Figure 1). To guarantee the reliability of the predicted results, a very fine mesh (minimum element size 10 nm) was utilized in proximity of the region where the AFM bead comes in contact with the cell. The AFM tip was hypothesized, according to the experiments carried out and previously described, to indent the cell in its highest point; an indentation depth of $\delta = 200$ nm was imposed to the indenter along the vertical direction. Following previous studies [16,31], the contact between the cell and the AFM bead was assumed to be frictionless. Symmetry constraints were imposed to the faces of the model lying on the symmetry planes π_1 and π_2 (Figure 1). Stress fibers were simulated as pre-tensioned cables with a cross-sectional area of $0.05 \mu\text{m}^2$ [43,44], a Young's modulus of 300 kPa [43], subjected to a tensile force of 10 nN [45,46]. These cables were hypothesized to exert only tensile forces; to this purpose, the option 'no compression' was enabled so that no compressive stress was allowed. Three types of stress fibers were simulated: ventral stress fibers (highlighted in green, Figure 2), dorsal stress fibers (highlighted in red, Figure 2), and transverse arcs (highlighted in blue, Figure 2). Following Vassaux and Milan [47], Rogge et al. [48] and Nagayama and Matsumoto [49], nine stress fibers were modeled in the simplified one-quarter model. In detail, the dorsal stress fibers connect the nodes of the upper region of the cell cortex to nodes of the lower region of the cell cortex (Figure 2) located in proximity of the substrate. The ventral stress fibers, instead, are practically parallel to the plane where the cell lies and connect nodes of the cell cortex located in proximity of the substrate (Figure 2) [36]. The focal adhesions anchoring the dorsal and the ventral stress fibers to the substrate were simulated by including constraints at the bottom cell surface preventing any relative displacement between the cell and the substrate. The transverse arcs, which do not directly attach to focal adhesions [50], connect circumferentially the dorsal stress fibers (Figure 2).

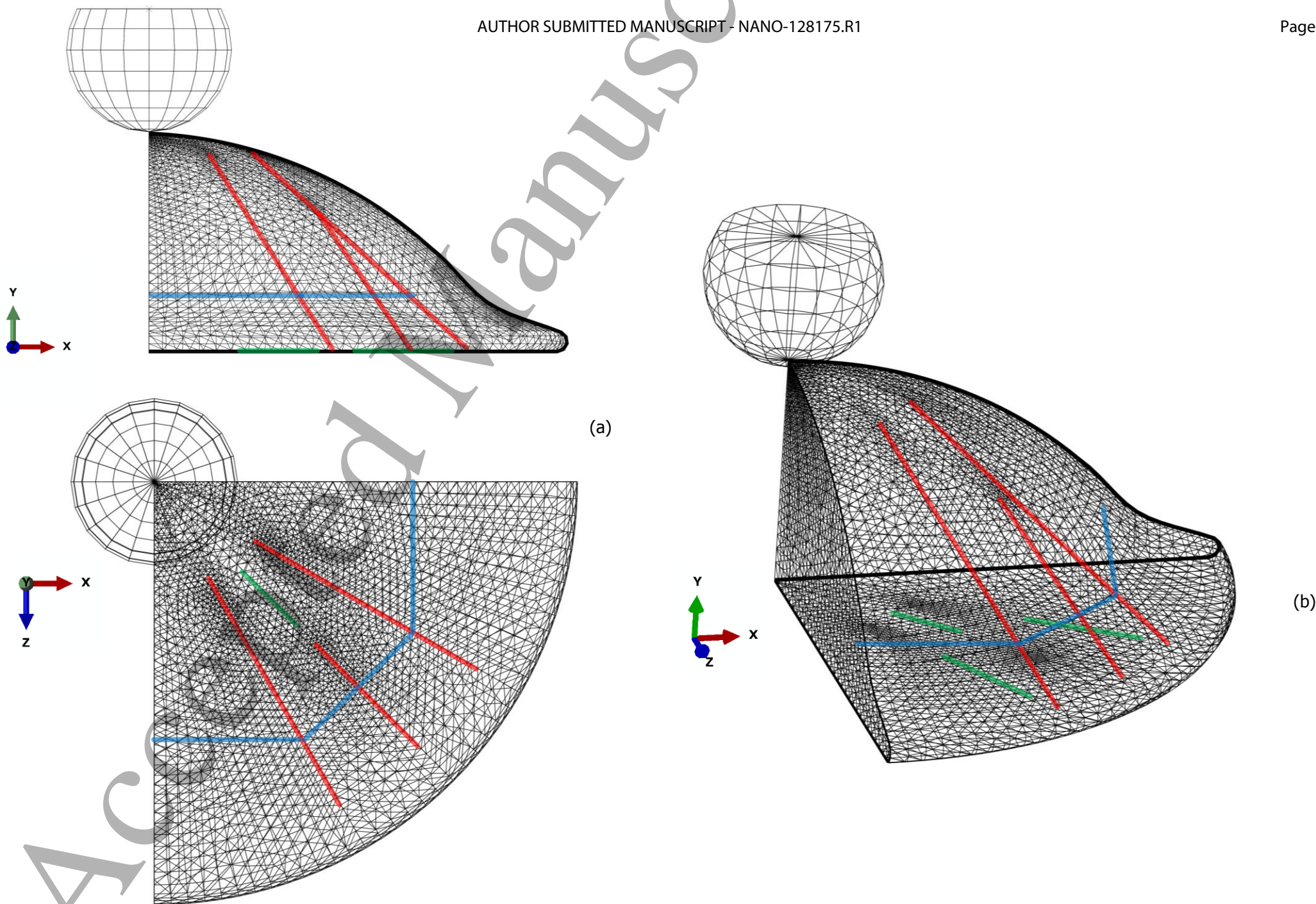


Figure 2. Orthographic representations (a) and axonometric view (b) of the cell model with stress fibers. The model includes dorsal stress fibers (highlighted in red), ventral stress fibers (highlighted in green) and transverse arcs (highlighted in blue) that were modelled as no-compression pre-tensioned cables.

Given that the cell mechanical properties are orders of magnitude smaller than those of the AFM bead, we modeled the indenter as a rigid spherical surface with a 5 μm radius, which is the same radius of the indenter utilized in the experiments above described. Following a previous study [19] all the three (i.e. the cytoskeleton, the cortex, and the nucleus) cellular subcomponents were modeled as hyperelastic materials. In detail, the Arruda-Boyce constitutive law was implemented since it is well suited for modeling incompressible materials. This law describes the strain energy function as a function of two constants, the shear modulus μ_{8chain} and the distensibility λ_L . Further details on the Arruda-Boyce hyperelastic constitutive model are reported in a previous study [16]. The Young's modulus E_{AB} associated to this hyperelastic constitutive law is given by:

$$E_{AB} = 2(1 + \nu)\mu_{8chain} \quad (1)$$

being ν the Poisson's ratio that, to account for material incompressibility, can be set equal to 0.4999.

The specific values given to the shear modulus and to the distensibility of the cytoskeleton (i.e. μ_{8chain_cyto} and λ_{L_cyto} , respectively) and the cell cortex (i.e. μ_{8chain_cortex} and λ_{L_cortex} , respectively) of the nanoindented MSCs were determined via the optimization algorithm described below. The hyperelastic parameters for the nucleus were $\mu_{8chain_nucleus} = 12000$ Pa and $\lambda_{L_nucleus} = 3.07$, where the nucleus shear modulus corresponds approximately, to the average value of the cell cytoskeletons material properties (the average was computed over the ten stem cells investigated) obtained with the optimization algorithm for the ten cell samples, increased by one order of magnitude, while the nucleus distensibility corresponds

1
2
3 to the average value of the distensibility predicted for the ten cells. Indeed, the proposed
4 optimization algorithm, due to the large distance between the AFM tip and the nucleus, was
5 not capable to extract the nucleus material properties. Therefore, as proposed in Deguchi et
6 al. [51], we hypothesized that the nucleus material properties are approximately one order of
7 magnitude larger than those computed for the other cell components.
8
9
10
11
12
13
14
15

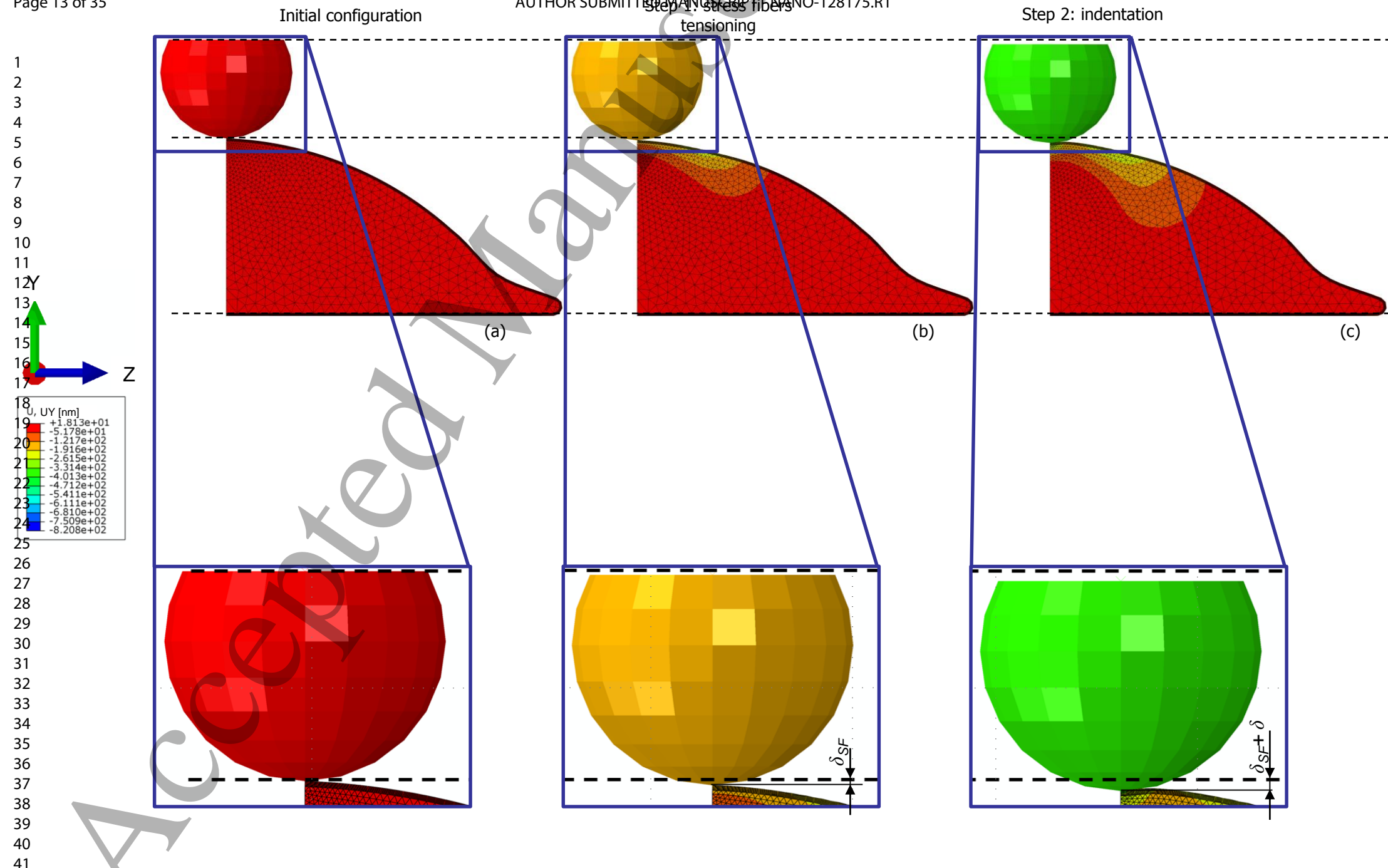
16 2.5. *Finite element analyses*

17
18
19
20
21 Two-step nonlinear finite element analyses were carried out. In the first step, the tensioning
22 of the stress fibers was simulated: a tensile force of 10 nN was applied to the stress fibers.
23 Due to the action of the stress fibers, the upper region of the cell experiences a localized
24 vertical displacement δ_{SF} (with respect to the initial configuration, Figure 3) which is in the
25 nanometer range. The deformed cell configuration resulting from the stress fibers tensioning
26 represents the starting configuration for the second step, in which the force exerted by the
27 stress fibers was kept constant while a nanoindentation of $\delta = 200$ nm was imposed to the
28 AFM bead. At the end of the entire analysis the upper region of the cell experienced a total
29 vertical displacement:
30
31
32
33
34
35
36
37
38
39
40
41

$$42 \quad \delta_{TOT} = \delta_{SF} + \delta \quad (2)$$

43
44 The modeling strategy of the two-step finite element analysis was adopted to simulate what
45 occurs *in vitro* where a given stem cell that is attached to a substrate – and hence is subjected
46 to the tensile forces of adhesive structures acting on it (initial condition simulated in the first
47 step) – is subjected to nanoindentation measurements (second step).
48
49
50
51
52
53
54

55 2.6. *Optimization algorithm for mesenchymal stem cell characterization*



42 **Figure 3.** A two-step nonlinear finite element analysis was carried out. In the first step (b) the tensioning of the stress fibers was simulated: a tensioning force of 10 nN was applied to each of the
43 modelled stress fibers. In the second step (c), the force exerted by stress fibers was kept constant while a nanoindentation of $\delta = 200$ nm was imposed to the AFM bead. The three dashed lines were
44 shown as a reference. In the first step, due to the action of the stress fibers, the cell experiences a vertical displacement δ_{SF} (with respect to the initial configuration (a)) which is in the nanometer
45 range. At the end of the entire analysis the cell experiences a total vertical displacement $\delta_{TOT} = \delta_{SF} + \delta$

1
2
3
4
5
6 The finite element model described above was incorporated within an optimization algorithm
7
8 coded in Matlab® environment and utilized to characterize the cell mechanical properties
9
10 (Figure 4), i.e. to determine the specific values of μ_{8chain} and λ_L for the ten nanoindented
11
12 MSCs. Generally speaking, the algorithm compares the force-indentation curve
13
14 experimentally retrieved (Blocks {0} and {1}, Figure 4) with that numerically predicted and
15
16 perturbs the material properties (implemented in the cell finite element model) many times
17
18 until the difference between the two curves is minimized thus becoming smaller than an *a-*
19
20 *priori* fixed quantity ε .
21
22

23
24 The algorithm first asks the user to initialize the cell material properties to be
25
26 implemented in the finite element model, (Block {2}, Figure 4). Then, it acquires the value
27
28 specified by the user (Block {3}, Figure 4), applies the boundary conditions (Block {4},
29
30 Figure 4), the tensile force on stress fibers, and runs the first step of the analysis (Block {5},
31
32 Figure 4). At the end of the first step, the algorithm reads the value of the displacement δ_{SF}
33
34 experienced by the highest point of the cell and computes δ_{TOT} according to the Equation (4)
35
36 (Block {6}, Figure 4). Therefore, the second step starts, where an indentation depth equal to
37
38 δ_{TOT} is imposed to the spherical AFM tip (Block {7}, Figure 4). (Note: Abaqus refers the
39
40 nanoindentation depth not to the current position occupied by the model but to its initial
41
42 configuration. For this reason, we imposed an indentation depth δ_{TOT} that is the sum of the
43
44 displacement experienced by the cell in the first step and the indentation depth $\delta = 200$ nm
45
46 that we want to impose on the cell). Then, the algorithm extracts the numerical force-
47
48 indentation curve (Block {8}, Figure 4), multiplies the values of the force by four to account
49
50 for the use of the simplified one-quarter model and compares the resulting numerical curve
51
52
53
54
55
56
57
58
59
60

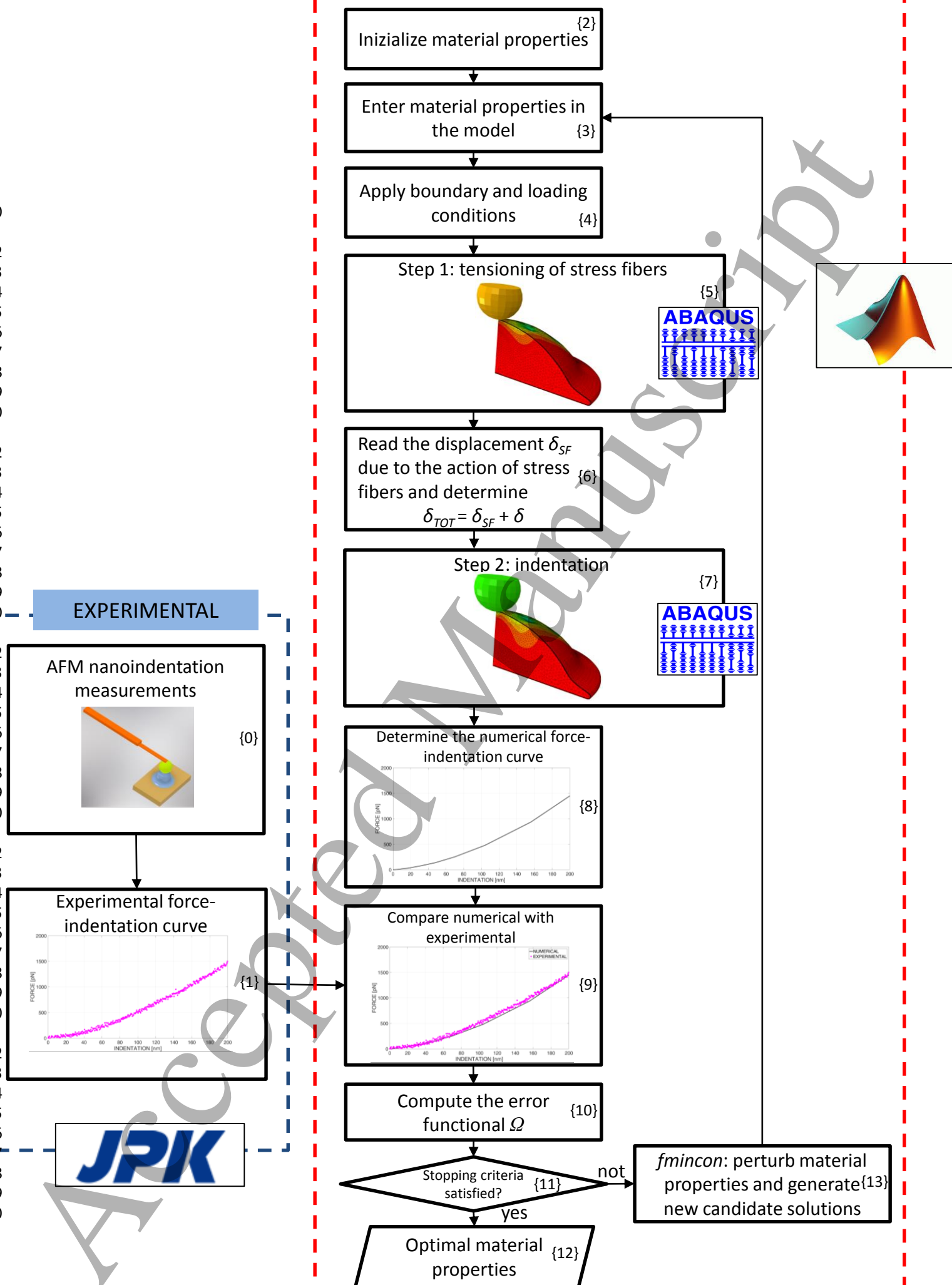


Figure 4. Scheme of the optimization algorithm implemented to determine the material properties of the ten cell samples investigated.

1
2
3 with the experimental one (Block {9}, Figure 4). Based on the least square method, the
4 optimization algorithm attempts to identify the optimal hyperelastic properties of the
5 cytoskeleton and the cell cortex. Further details on the error functional Ω minimized by the
6 algorithm (Block {10}, Figure 4) and the lower and the upper bounds fixed in the
7 optimization process are reported in a previous study [19].
8
9

10
11
12
13
14
15 After computing the error functional Ω , the algorithm verifies if the stopping criteria –
16 that depend, in turn, on the tolerance values initially fixed by the user – are satisfied (Block
17 {11}, Figure 4). If so, the algorithm stops and gives in output the optimal material properties
18 of the cytoskeleton and the cell cortex (Block {12}, Figure 4). If not, the algorithm perturbs
19 the cytoskeleton and the cortex material properties generating new candidate solutions and
20 starting a new optimization cycle (Block {13}, Figure 4).
21
22
23
24
25
26
27

28
29 This algorithm was utilized to characterize the mechanical behavior of the ten indented
30 cells. In other words, for each of the ten investigated cells, five force-indentation curves were
31 taken in the highest point, the average curve was computed that, in turn, was utilized in the
32 algorithm (Blocks {0} and {1}) to predict the material properties of the ten cells.
33
34
35
36
37

38 To assess the effect of adhesive structures on nanoindentation measurements, the
39 optimization algorithm was changed accordingly and utilized to characterize the cell material
40 in the case the adhesive structures are not taken into account. Practically, this new algorithm
41 is the same as that shown in Figure 4 with the only difference that it does not include the
42 Blocks {5} and {6}, i.e. the Blocks regarding the tensioning of stress fibers. In other words,
43 in this new algorithm, the finite element analyses included just one step: indentation.
44
45
46
47
48
49
50

51 All the computations were performed on an HP XW6600-Intel® Xeon® Dual-Processor
52 E5-5450 3 GHz – 32 Gb RAM. Each optimization process required to run approximately at
53
54
55
56 least 70 cycles (and hence 70 finite element analyses) to find the optimal material properties.
57
58
59
60

1
2
3 Considering that each analysis had a duration of about 4 hours in the case of the model
4 including the adhesive structures and about 3 hours in the case of the model neglecting them
5
6 and that ten cell samples were investigated, it follows that a total of 70 (# of cycles/analyses)
7
8 $\times 4$ (duration of each analysis, adhesive structures included) $\times 10$ (# of cell samples
9
10 investigated) $+ 70$ (# of cycles/analyses) $\times 3$ (duration of each analysis, adhesive structures
11
12 excluded) $\times 10$ (# of cell samples investigated) = 4900 hours was required to complete the
13
14 analyses carried out in this study.
15
16
17
18
19

20 **3. Results**

21
22
23
24
25
26 Implementing the above-described optimization algorithm, the optimal material properties of
27
28 cytoskeleton and cortex were determined for all the ten cell samples indented. The material
29
30 properties of the indented cells were also computed by implementing the Hertz contact
31
32 theory. Tables 1 and 2 list the obtained results in both cases, adhesive structures included in
33
34 the model and adhesive structures not taken into account, respectively. The last line in both
35
36 tables report the average \pm standard deviation of the ten cell samples investigated in this
37
38 study. Interestingly, we observed that neglecting the effect of adhesive structures on
39
40 nanoindentation measurements leads to underestimate the value of the shear stress and hence
41
42 of the Young's modulus E_{AB} associated with the Arruda-Boyce constitutive law (Equation
43
44 (3)). We computed the percent difference between the material properties predicted in the
45
46 absence of adhesive structures and those predicted in the presence of them as:
47
48
49
50
51
52
53
54
55
56
57
58
59
60

Table 1. Optimal hyperelastic properties predicted for the ten cell samples, in the case of adhesive structures included in the model.

	Cytoskeleton μ_{chain_cyto} [Pa]	Cytoskeleton λ_{L_cyto}	Cortex μ_{chain_cortex} [Pa]	Cortex λ_{L_cortex}	Cytoskeleton E_{AB_cyto} [Pa]	Cortex E_{AB_cortex} [Pa]	E_H [Pa]
Sample 1	1173.014	3.063	3251.228	3.070	3519.041	9753.683	4110.000
Sample 2	1763.387	3.065	3229.130	3.070	5290.161	9687.391	6350.000
Sample 3	1487.424	3.022	3223.649	3.070	4462.273	9670.946	5200.000
Sample 4	858.358	3.070	3245.838	3.085	2575.074	9737.515	3195.000
Sample 5	752.610	3.093	3214.918	3.091	2257.831	9644.755	2800.000
Sample 6	967.037	3.093	3190.000	3.092	2901.112	9570.000	3410.000
Sample 7	1545.920	3.073	3269.109	3.072	4637.760	9807.327	5550.000
Sample 8	1517.130	3.022	3243.060	3.067	4551.390	9729.180	5680.000
Sample 9	1043.050	3.077	3185.068	3.121	3129.150	9555.204	3455.000
Sample 10	880.026	3.075	3205.980	3.087	2640.078	9617.940	3050.000
average \pm s.d.	1198.796 \pm 352.630	3.065 \pm 0.025	3225.798 \pm 27.263	3.083 \pm 0.016	3596.387 \pm 1057.888	9677.394 \pm 81.789	4280.000 \pm 1293.194

Table 2. Optimal hyperelastic properties predicted for the ten cell samples, in the case of adhesive structures excluded from the model.

	Cytoskeleton μ_{8chain_cyto} [Pa]	Cytoskeleton λ_{L_cyto}	Cortex μ_{8chain_cortex} [Pa]	Cortex λ_{L_cortex}	Cytoskeleton E_{AB_cyto} [Pa]	Cortex E_{AB_cortex} [Pa]
Sample 1	1067.818	3.060	3242.611	3.088	3203.454	9727.833
Sample 2	1656.340	3.070	3201.720	3.085	4969.021	9605.160
Sample 3	1385.048	3.042	3201.467	3.100	4155.143	9604.401
Sample 4	749.359	3.083	3234.576	3.091	2248.076	9703.729
Sample 5	637.246	3.093	3230.370	3.092	1911.739	9691.110
Sample 6	830.987	3.099	3239.491	3.093	2492.962	9718.473
Sample 7	1478.820	3.050	3240.000	3.072	4436.460	9720.000
Sample 8	1446.368	3.027	3241.850	3.068	4339.104	9725.550
Sample 9	916.168	3.094	3194.001	3.097	2748.504	9582.003
Sample 10	802.672	3.092	3214.900	3.091	2408.016	9644.700
average \pm s.d.	1097.083 \pm 363.142	3.071 \pm 0.025	3224.099 \pm 19.149	3.088 \pm 0.010	3291.248 \pm 1089.426	9672.296 \pm 57.447

percent difference [%]

$$= \frac{m.p.without_adhesive_structures - m.p.with_adhesive_structures}{m.p.with_adhesive_structures} \times 100 \quad (3)$$

being $m.p.without_adhesive_structures$, one of the material properties (i.e. one of the quantities: μ_{8chain_cyto} , λ_{L_cyto} , μ_{8chain_cortex} , λ_{L_cortex}) computed with the model neglecting the adhesive structures and $m.p.with_adhesive_structures$ the same quantity computed with the model including them. Small (positive or negative) values of this percent difference were found in the case of the parameters λ_{L_cyto} , μ_{8chain_cortex} and λ_{L_cortex} ; larger values, all negative, were instead computed, in the case of the shear modulus of the cytoskeleton μ_{8chain_cyto} (Figure 5(a)). Furthermore, we found that, while the distensibility values are very close for the cytoskeleton and the cortex, the shear modulus is significantly higher in the cortex than in the cytoskeleton (Tables 1 and 2). The Young's modulus E_H computed with the Hertz contact theory assumes intermediate values between the values E_{AB_cyto} (i.e. the Young's modulus associated to the hyperelastic constitutive law of Arruda-Boyce and computed for the cytoskeleton) and E_{AB_cortex} (i.e. the same quantity computed for the cortex) (Figure 5(b)).

The rather high correlation coefficient R^2 between the predicted and the experimental force-indentation curves in both cases, adhesive structures included (Figure 6) and excluded (Figure 7), demonstrated the reasonably good capability of the proposed model of reproducing the physics of the problem.

4. Discussion

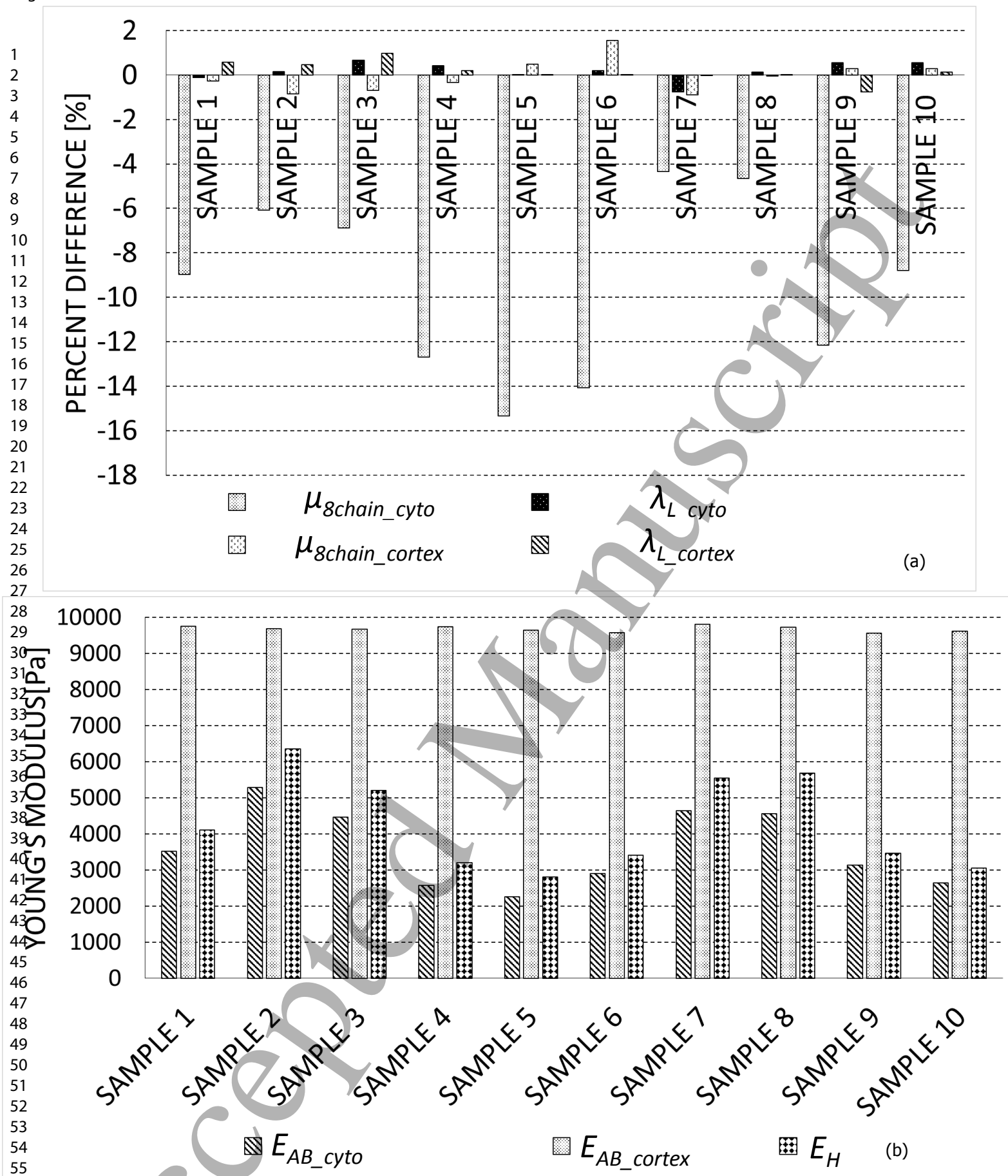


Figure 5. (a) Percent difference between the material properties computed in the presence and in the absence of adhesive structures. (b) Equivalent Young's modulus computed with the proposed optimization algorithm for each sample, compared with the material properties obtained via the Hertz contact theory.

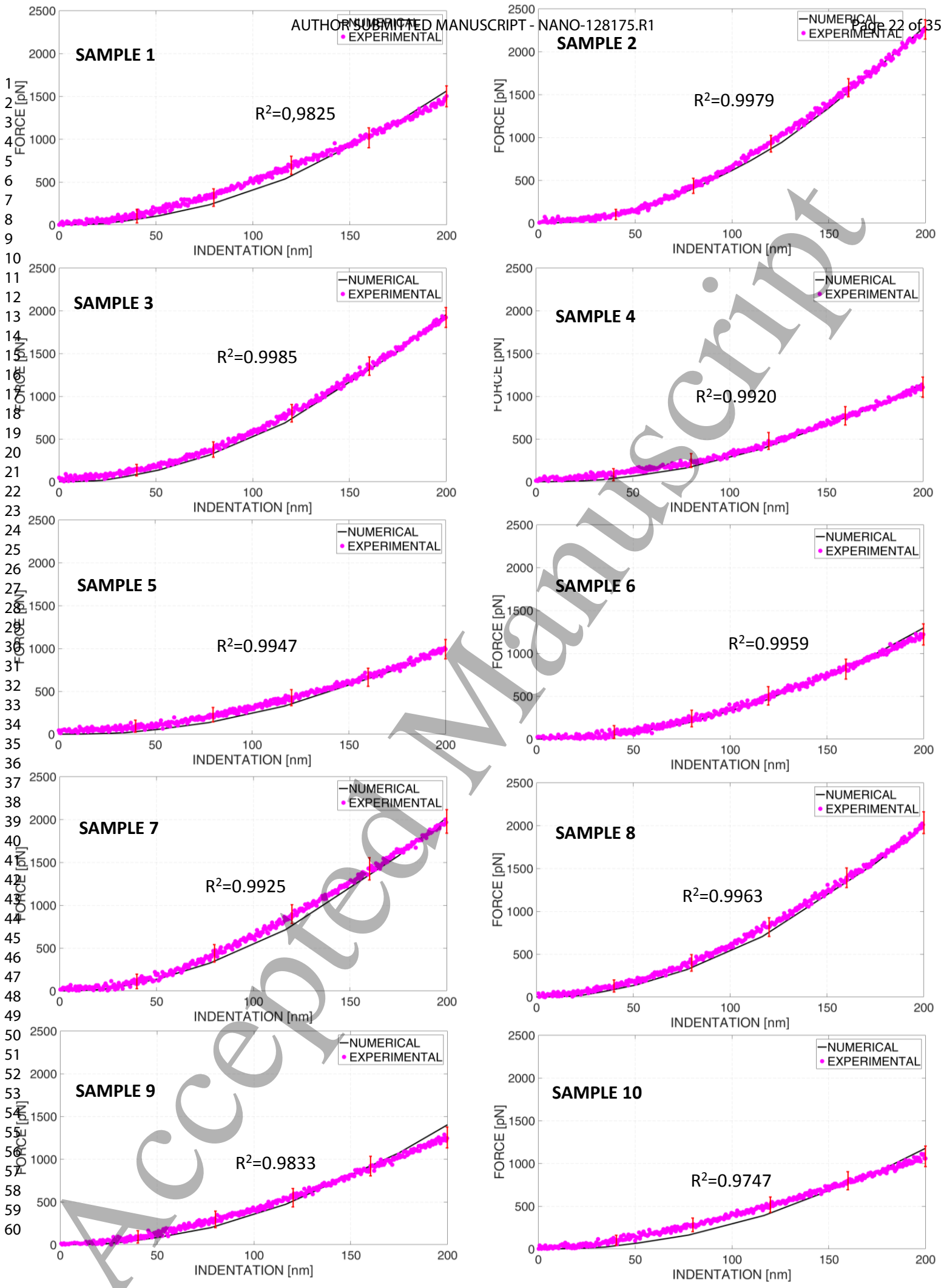


Figure 6. Comparison of force-indentation curves experimentally retrieved and numerically obtained with the optimization algorithm for the ten cell samples investigated: adhesive cell-substrate structures included in the model.

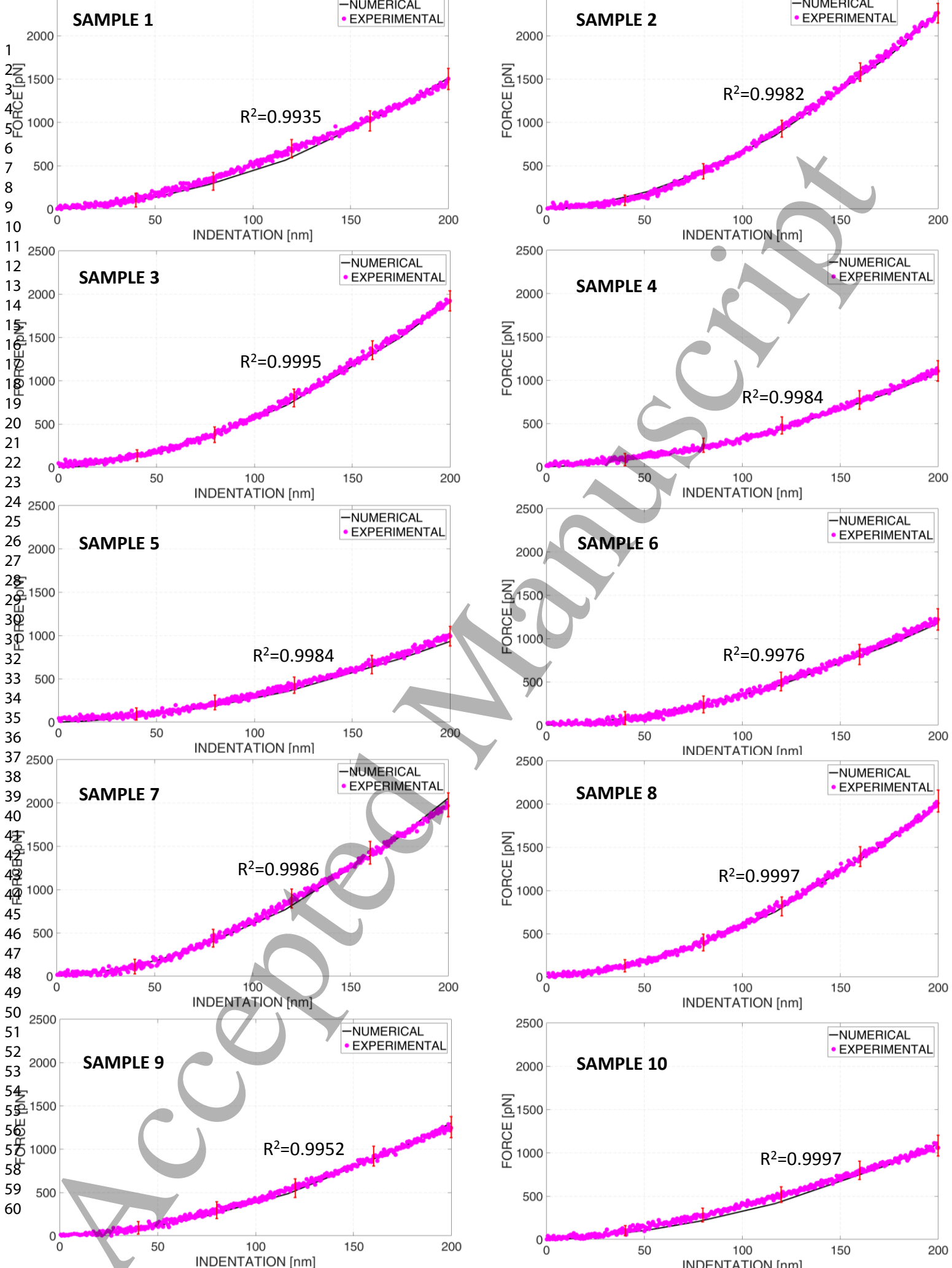


Figure 7. Comparison of force-indentation curves experimentally retrieved and numerically obtained with the optimization algorithm for the ten cell samples investigated: adhesive cell-substrate structures excluded from the model.

1
2
3 A computational framework was developed to characterize the mechanical behavior of
4 mesenchymal stem cells and to assess how these properties change if the adhesive structures
5 acting on the cells are taken into account or not.
6
7
8

9
10 The proposed model presents some limitations. First, only the cytoskeleton, the cell
11 cortex, and the nucleus were modeled. In reality, the subcellular components are much more
12 numerous than the three ones considered. However, the choice of modeling each of them and
13 especially those with very small dimensions would necessarily require the use of a very fine
14 mesh and hence a very large computational power. Increases in computational power will
15 ultimately allow simulating more realistically the cell mechanical behavior. Second, for each
16 nanoindented cell, an average – computed over the five nanoindentation measurements –
17 experimental force-indentation curve was considered and utilized as a reference in the
18 optimization algorithm. Another possible approach consists in considering each of the five
19 experimental force-indentation curves, implementing the optimization algorithm on each of
20 them and determining the global cell mechanical properties as the average value of the five
21 obtained values. Preliminary analyses revealed that adopting such a strategy leads to results
22 very close to those obtained by considering the average experimental force-indentation curve.
23 For instance, the standard deviation of the mechanical properties obtained considering each
24 individual experimental curve for the cell sample 3, does not exceed 195 Pa for E_{AB_cyto} and
25 9 Pa for the E_{AB_cortex} . These values are one order of magnitude smaller than the standard
26 deviation values (Table 1 and Table 2) obtained for the ten cell samples investigated in this
27 study. Furthermore, the average value obtained considering each individual experimental
28 force-indentation curve differs from that obtained by considering the average of the five
29 experimental curves by less than 0.5% in the case of the cytoskeleton and by less than 0.2%
30 in the case of the cortex. These results led us to adopt the less expensive procedure – from
31
32
33
34
35
36
37
38
39
40
41
42
43
44
45
46
47
48
49
50
51
52
53
54
55
56
57
58
59
60

1
2
3 the computational point of view – utilized in previous studies [15,16] based on the use of the
4 average experimental force-indentation curve. Third, the nucleus was not characterized.
5
6 Material properties approximately one order of magnitude larger than those of the cell
7 cytoskeleton were hypothesized but a direct “measurement” of the nucleus material
8 properties is missing. To characterize the nucleus, the AFM tip should indent more deeply
9 the cell thus approaching more closely the nucleus. This poses two issues from both, the
10 physical and the computational point of view. From the physical point of view, it is likely
11 that a deep indentation would damage the cell. From the computational point of view, the
12 simulation of deep nanoindentations raises many issues of convergence of the finite element
13 analysis. Convergence is all the more problematic the greater the depth of indentation.
14
15 Studies aiming at addressing these aspects should be carried out in the future. However,
16 preliminary analyses revealed that the predicted cell material properties are practically not
17 affected – or are influenced in a very marginal way – by the specific values hypothesized for
18 the nucleus mechanical properties. For instance, the force predicted at the indentation depth
19 of 200 nm for the cell sample 3 by setting the nucleus properties to twice ($\mu_{8chain_nucleus} =$
20 24000 Pa and $\lambda_{L_nucleus} = 3.07$) and half ($\mu_{8chain_nucleus} = 6000$ Pa and $\lambda_{L_nucleus} = 3.07$) the
21 hypothesized values ($\mu_{8chain_nucleus} = 12000$ Pa and $\lambda_{L_nucleus} = 3.07$) differs from that predicted
22 for the design hypotheses by less than 0.21%. As a consequence of this, the dispersion of
23 results deriving from the use of different nucleus mechanical properties, is approximately
24 two orders of magnitude smaller than that existing between the ten cell samples investigated
25 (Table 1 and 2).

26
27 However, in spite of these limitations, the proposed computational framework predicts
28 cell material properties that are consistent with those reported in the literature. Chen et al.
29
30
31
32
33
34
35
36
37
38
39
40
41
42
43
44
45
46
47
48
49
50
51
52
53
54
55
56
57
58
59
60

[24] determined by atomic force microscopy and implementing the Hertz contact theory, an average Young's modulus of amniotic fluid-derived stem cells of 3.97 ± 0.53 kPa. Kiss et al. [21], characterized with AFM the material properties of human embryonic stem cells and found that the Young's modulus ranges in the interval $[0.05 \div 10]$ kPa. Liang et al. [23] found, using atomic force microscopy, that after 14 days of culture, the modulus of mesenchymal stem cells cultured in osteogenic medium is approximately 3.5 kPa. These values are consistent with those measured with the proposed approach and, in particular, are overlapping with the values of E_{AB} determined for the ten cell samples investigated (Figure 5(b)). Interestingly, the values of the Young's modulus (E_H , Table 1) computed with the Hertz's contact theory are, in all the cell samples investigated, smaller than E_{AB_cortex} and greater than E_{AB_cyto} . In detail, the computed values of E_H are closer to E_{AB_cyto} than to E_{AB_cortex} , which is consistent with our expectations, being the cytoskeleton the "principal" material included in the cell.

The results of this study demonstrate that neglecting the adhesion structures acting on cells attached to the substrate leads to underestimate the material properties. This means that if the cell adhesive structures are not considered, errors up to 15%, in the evaluation of the material properties, can be made. This result can be explained considering how the force-indentation curve changes if, for the same material properties, adhesive structures are considered or not (Figure 8). Interestingly, including the adhesive structures leads to obtain smaller values of the force with which the AFM tip indents the cell. The tensioning of the stress fibers creates a tensile pre-stress state within the upper part of the cell that facilitates the penetration of the indenter and that "diminishes" the resistance opposed by the cell material to contrast the compression imposed during indentation. In other words, when the

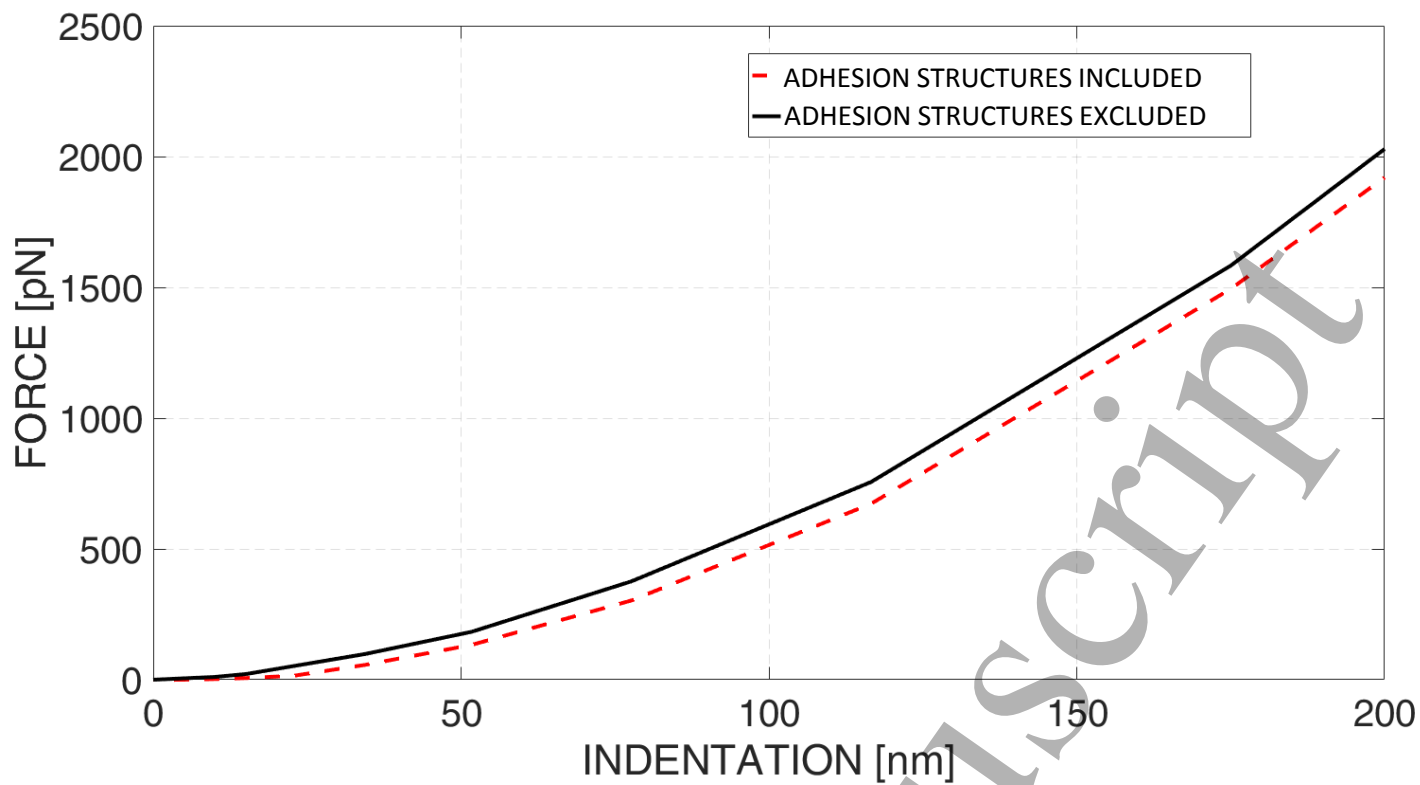


Figure 8. Comparison between the force-indentation curves obtained for the same material properties and computed by the optimization algorithm including and excluding the adhesion structures action.

1
2
3 adhesive structures are simulated, it is possible to notice that the overall work to deform the
4 cell until it reaches a final deformed state, is partially done from the adhesive structures and
5 partially done by the AFM tip, when, conversely, these are not simulated, the entire work to
6 indent the cell must be done from the AFM tip. This leads, if the adhesive structures are not
7 taken into account, to an apparent reduction of the cell material properties (Table 1 and Table
8 2).

9
10
11
12
13
14
15
16
17 The proposed computational framework presents important advantages with respect to
18 the approach traditionally utilized to extract, from the force-indentation curve, the cell
19 material properties. The framework, in fact, permits to separately determine the material
20 properties of subcellular components with just “one” indentation measurement.
21 Hypothetically, to determine through the traditional approach based on the Hertz contact
22 theory the material properties of each subcellular component, one should first separate it
23 physically from the cell context and successively subject it to nanoindentation, which is a
24 very complex or even impossible procedure to carry out. Conversely, with the proposed
25 algorithm, without separating the cytoskeleton and the cell cortex from the entire cell, it is
26 possible to distinctly determine their material properties.

5. Conclusions

27
28
29
30
31
32
33
34
35
36
37
38
39
40
41
42
43
44
45
46
47
48
49 In conclusion, we developed a computational framework that allows determining how the
50 material properties of mesenchymal stem cells change if the adhesion of cell-substrate
51 structures is considered or not. To this purpose, a model simulating the action of focal
52 adhesions and stress fibers was developed. In general, we found that neglecting the adhesive

1
2
3 structures acting on stem cells being subjected to nanoindentation leads to underestimate the
4 cell material properties. The error of assessment committed if adhesive structures are not
5 taken into account can be substantial and up to 15%. This leads us to conclude that the effect
6 of adhesive structures cannot be overlooked especially for cells that include a large number
7 of adhesive structures.
8
9
10
11
12
13
14
15
16
17

18 **Acknowledgments**

19
20
21
22
23 We gratefully acknowledge the support given by Dr. Patrick Horn from the Department of
24 Medicine V, Heidelberg University, for donating the hMSCs. We thank also: (a) the
25 European Union's Framework Program for Research and Innovation Horizon 2020 (2014 -
26 2020) under the Marie Skłodowska-Curie Grant Agreement No. 658334; (b) the Italian
27 Ministry of Education, University and Research under the Programme: (1) PON R&I 2014 -
28 2020 and FSC (Project "CONTACT", ARS01_01205); (2) "Department of Excellence"
29 Legge 232/2016 (Grant No. CUP - D94I18000260001), for the fundings received.
30
31
32
33
34
35
36
37
38
39
40
41

42 **References**

- 43
44
45 [1] Kuznetsova T G, Starodubtseva M N, Yegorenkov N I, Chizhik S A and Zhdanov R
46 I 2007 Atomic force microscopy probing of cell elasticity *Micron* **38** 824–33
47
48 [2] Marcotti S, Reilly G C and Lacroix D 2019 Effect of cell sample size in atomic
49 force microscopy nanoindentation *J. Mech. Behav. Biomed. Mater.* **94** 259–66
50
51 [3] Vichare S, Inamdar M M and Sen S 2012 Influence of cell spreading and
52 contractility on stiffness measurements using AFM *Soft Matter* **8** 10464–71
53
54 [4] Boccaccio A, Papi M, De Spirito M, Lamberti L and Pappalettere C 2013 Effect of
55 the residual stress on soft sample nanoindentation *Appl. Phys. Lett.* **102** 1–5
56
57
58
59
60

- 1
2
3 [5] Boccaccio A, Lamberti L, Papi M, De Spirito M and Pappalettere C 2015 Effect of
4 AFM probe geometry on visco-hyperelastic characterization of soft materials
5 *Nanotechnology* **26** 325701
6
7 [6] Pesen D and Hoh J H 2005 Micromechanical architecture of the endothelial cell
8 cortex *Biophys. J.* **88** 670–9
9
10 [7] Rosenbluth M J, Lam W A and Fletcher D A 2006 Force microscopy of
11 nonadherent cells: A comparison of leukemia cell deformability *Biophys. J.* **90**
12 2994–3003
13
14 [8] Murakoshi M, Yoshida N, Iida K, Kumano S, Kobayashi T and Wada H 2006 Local
15 mechanical properties of mouse outer hair cells: Atomic force microscopic study
16 *Auris Nasus Larynx* **33** 149–57
17
18 [9] Zhang J S, Kraus W E and Truskey G A 2004 Stretch-induced nitric oxide
19 modulates mechanical properties of skeletal muscle cells *Am. J. Physiol. - Cell*
20 *Physiol.* **287** 292–9
21
22 [10] Lieber S C, Aubry N, Pain J, Diaz G, Kim S J and Vatner S F 2004 Aging increases
23 stiffness of cardiac myocytes measured by atomic force microscopy nanoindentation
24 *Am. J. Physiol. - Hear. Circ. Physiol.* **287** 645–51
25
26 [11] Ciasca G, Papi M, Di Claudio S, Chiarpotto M, Palmieri V, Maulucci G, Nocca G,
27 Rossi C and De Spirito M 2015 Mapping viscoelastic properties of healthy and
28 pathological red blood cells at the nanoscale level *Nanoscale* **7** 17030–7
29
30 [12] Dulińska I, Targosz M, Strojny W, Lekka M, Czuba P, Balwierz W and Szymoński
31 M 2006 Stiffness of normal and pathological erythrocytes studied by means of
32 atomic force microscopy *J. Biochem. Biophys. Methods* **66** 1–11
33
34 [13] Wozniak M J, Kawazoe N, Tateishi T and Chen G 2010 Change of the mechanical
35 properties of chondrocytes during expansion culture *Soft Matter* **6** 2462–9
36
37 [14] Dittmann J, Dietzel A and Böhl M 2018 Mechanical characterisation of oocytes - The
38 influence of sample geometry on parameter identification *J. Mech. Behav. Biomed.*
39 *Mater.* **77** 764–75
40
41 [15] Boccaccio A, Lamberti L, Papi M, De Spirito M, Douet C, Goudet G and
42 Pappalettere C 2014 A hybrid characterization framework to determine the visco-
43 hyperelastic properties of a porcine zona pellucida *Interface Focus* **4**
44
45 [16] Boccaccio A, Frassanito M C, Lamberti L, Brunelli R, Maulucci G, Monaci M, Papi
46 M, Pappalettere C, Parasassi T, Sylla L, Ursini F and De Spirito M 2012 Nanoscale
47 characterization of the biomechanical hardening of bovine zona pellucida *J. R. Soc.*
48 *Interface* **9** 2871–82
49
50 [17] Palmieri V, Lucchetti D, Maiorana A, Papi M, Maulucci G, Calapà F, Ciasca G,
51 Giordano R, Sgambato A and De Spirito M 2015 Mechanical and structural
52 comparison between primary tumor and lymph node metastasis cells in colorectal
53 cancer *Soft Matter* **11** 5719–26
54
55
56
57
58
59
60

- 1
2
3 [18] Palmieri V, Lucchetti D, Maiorana A, Papi M, Maulucci G, Ciasca G, Svelto M, De
4 Spirito M and Sgambato A 2014 Biomechanical investigation of colorectal cancer
5 cells *Appl. Phys. Lett.* **105**
6
- 7 [19] Boccaccio A, Uva A E, Papi M, Fiorentino M, De Spirito M and Monno G 2017
8 Nanoindentation characterisation of human colorectal cancer cells considering cell
9 geometry, surface roughness and hyperelastic constitutive behaviour
10 *Nanotechnology* **28** 1–18
11
- 12 [20] Zhou Z L, Ngan A H W, Tang B and Wang A X 2012 Reliable measurement of
13 elastic modulus of cells by nanoindentation in an atomic force microscope *J. Mech.*
14 *Behav. Biomed. Mater.* **8** 134–42
15
- 16 [21] Kiss R, Bock H, Pells S, Canetta E, Adya A K, Moore A J, De Sousa P and
17 Willoughby N A 2011 Elasticity of human embryonic stem cells as determined by
18 atomic force microscopy *J. Biomech. Eng.* **133** 1–10
19
- 20 [22] Nikolaev N I, Müller T, Williams D J and Liu Y 2014 Changes in the stiffness of
21 human mesenchymal stem cells with the progress of cell death as measured by
22 atomic force microscopy *J. Biomech.* **47** 625–30
23
- 24 [23] Liang X, Shi X, Ostrovidov S, Wu H and Nakajima K 2016 Probing stem cell
25 differentiation using atomic force microscopy *Appl. Surf. Sci.* **366** 254–9
26
- 27 [24] Chen Q, Xiao P, Chen J N, Cai J Y, Cai X F, Ding H and Pan Y L 2010 AFM
28 studies of cellular mechanics during osteogenic differentiation of human amniotic
29 fluid-derived stem cells *Anal. Sci.* **26** 1033–7
30
- 31 [25] Van der Meulen M C H and Huiskes R 2002 Why mechanobiology? A survey
32 article *J. Biomech.* **35** 401–14
33
- 34 [26] Boccaccio A, Ballini A, Pappalettere C, Tullo D, Cantore S and Desiate A 2011
35 Finite element method (FEM), mechanobiology and biomimetic scaffolds in bone
36 tissue engineering *Int. J. Biol. Sci.* **7** 112–32
37
- 38 [27] Ballini A, Boccaccio A, Saini R, Van Pham P and Tatullo M 2017 Dental-derived
39 stem cells and their secretome and interactions with Bioscaffolds/Biomaterials in
40 regenerative medicine: From the in vitro research to translational applications *Stem*
41 *Cells Int.* **2017** Article ID 6975251
42
- 43 [28] Cantore S, Crincoli V, Boccaccio A, Uva A E, Fiorentino M, Monno G, Bollero P,
44 Derla C, Fabiano F, Ballini A and Santacroce L 2018 Recent Advances in Endocrine,
45 Metabolic and Immune Disorders: Mesenchymal Stem Cells (MSCs) and Engineered
46 Scaffolds *Endocrine, Metab. Immune Disord. - Drug Targets* **18** 466–9
47
- 48 [29] Ballini A, Cantore S, Scacco S, Coletti D and Tatullo M 2018 Mesenchymal stem
49 cells as promoters, enhancers, and playmakers of the translational regenerative
50 medicine 2018 *Stem Cells Int.* **2018** Article ID 6927401
51
- 52 [30] Liu K K 2006 Deformation behaviour of soft particles: A review *J. Phys. D. Appl.*
53 *Phys.* **39**
54
55
56
57
58
59
60

- [31] Lin D C, Shreiber D I, Dimitriadis E K and Horkay F 2009 Spherical indentation of soft matter beyond the Hertzian regime: Numerical and experimental validation of hyperelastic models *Biomech. Model. Mechanobiol.* **8** 345–58
- [32] Gavara N and Chadwick R S 2016 Relationship between cell stiffness and stress fiber amount, assessed by simultaneous atomic force microscopy and live-cell fluorescence imaging *Biomech. Model. Mechanobiol.* **15** 511–23
- [33] Liu Y, Medda R, Liu Z, Galior K, Yehl K, Spatz J P, Cavalcanti-Adam E A and Salaita K 2014 Nanoparticle tension probes patterned at the nanoscale: Impact of integrin clustering on force transmission *Nano Lett.* **14** 5539–46
- [34] De Beer A G F, Cavalcanti-Adam E A, Majer G, Lopez-García M, Kessler H and Spatz J P 2010 Force-induced destabilization of focal adhesions at defined integrin spacings on nanostructured surfaces *Phys. Rev. E - Stat. Nonlinear, Soft Matter Phys.* **81** 1–7
- [35] Oria R, Wiegand T, Escribano J, Elosegui-Artola A, Uriarte J J, Moreno-Pulido C, Platzman I, Delcanale P, Albertazzi L, Navajas D, Trepát X, García-Aznar J M, Cavalcanti-Adam E A and Roca-Cusachs P 2017 Force loading explains spatial sensing of ligands by cells *Nature* **552** 219–24
- [36] BurrIDGE K and Guilluy C 2016 Focal adhesions, stress fibers and mechanical tension *Exp. Cell Res.* **343** 14–20
- [37] Livne A and Geiger B 2016 The inner workings of stress fibers - From contractile machinery to focal adhesions and back *J. Cell Sci.* **129** 1293–304
- [38] Vargas-Pinto R, Gong H, Vahabikashi A and Johnson M 2013 The effect of the endothelial cell cortex on atomic force microscopy measurements *Biophys. J.* **105** 300–9
- [39] Wagner W, Horn P, Castoldi M, Diehlmann A, Bork S, Saffrich R, Benes V, Blake J, Pfister S, Eckstein V and Ho A D 2008 Replicative senescence of mesenchymal stem cells: A continuous and organized process *PLoS One* **3**
- [40] Migliorini E, Horn P, Haraszti T, Wegner S V., Hiepen C, Knaus P, Richter R P and Cavalcanti-Adam E A 2017 Enhanced Biological Activity of BMP-2 Bound to Surface-Grafted Heparan Sulfate *Adv. Biosyst.* **1** 1–7
- [41] Vaiani L, Migliorini E, Cavalcanti-Adam E A, Uva A E, Fiorentino M, Gattullo M, Manghisi V M and Boccaccio A 2021 Coarse-grained elastic network modelling: A fast and stable numerical tool to characterize mesenchymal stem cells subjected to AFM nanoindentation measurements *Mater. Sci. Eng. C* **121** 111860
- [42] Su X, Zhou H, Bao G, Wang J, Liu L, Zheng Q, Guo M and Zhang J 2020 Nanomorphological and mechanical reconstruction of mesenchymal stem cells during early apoptosis detected by atomic force microscopy *Biol. Open* **9**
- [43] Kassianidou E and Kumar S 2015 A biomechanical perspective on stress fiber structure and function *Biochim. Biophys. Acta - Mol. Cell Res.* **1853** 3065–74

- 1
2
3 [44] Deguchi S and Sato M 2009 Biomechanical properties of actin stress fibers of non-
4 motile cells *Biorheology* **46** 93–105
5
6 [45] Deguchi S, Ohashi T and Sato M 2006 Tensile properties of single stress fibers
7 isolated from cultured vascular smooth muscle cells *J. Biomech.* **39** 2603–10
8
9 [46] Théry M, Pépin A, Dressaire E, Chen Y and Bornens M 2006 Cell distribution of
10 stress fibres in response to the geometry of the adhesive environment *Cell Motil.*
11 *Cytoskeleton* **63** 341–55
12
13 [47] Vassaux M and Milan J L 2017 Stem cell mechanical behaviour modelling:
14 substrate's curvature influence during adhesion *Biomech. Model. Mechanobiol.* **16**
15 1295–308
16
17 [48] Rogge H, Artelt N, Endlich N and Endlich K 2017 Automated segmentation and
18 quantification of actin stress fibres undergoing experimentally induced changes *J.*
19 *Microsc.* **268** 129–40
20
21 [49] Nagayama K and Matsumoto T 2010 Estimation of single stress fiber stiffness in
22 cultured aortic smooth muscle cells under relaxed and contracted states: Its relation
23 to dynamic rearrangement of stress fibers *J. Biomech.* **43** 1443–9
24
25 [50] Tojkander S, Gateva G and Lappalainen P 2012 Actin stress fibers - Assembly,
26 dynamics and biological roles *J. Cell Sci.* **125** 1855–64
27
28 [51] Deguchi S, Yano M, Hashimoto K, Fukamachi H, Washio S and Tsujioka K 2007
29 Assessment of the mechanical properties of the nucleus inside a spherical endothelial
30 cell based on microtensile testing *J. Mech. Mater. Struct.* **2** 1087–102
31
32
33
34
35
36
37
38
39
40
41
42
43
44
45
46
47
48
49
50
51
52
53
54
55
56
57
58
59
60

Figure legends

Figure 1. One-quarter finite element model of the nanoindented mesenchymal stem cell utilized in the study and detailed view of the cell region coming in contact with the AFM tip.

Figure 2. Orthographic representations (a) and axonometric view (b) of the cell model with stress fibers. The model includes dorsal stress fibers (highlighted in red), ventral stress fibers (highlighted in green) and transverse arcs (highlighted in blue) that were modelled as no-compression pre-tensioned cables.

Figure 3. A two-step nonlinear finite element analysis was carried out. In the first step (b) the tensioning of the stress fibers was simulated: a tensioning force of 10 nN was applied to each of the modelled stress fibers. In the second step (c), the force exerted by stress fibers was kept constant while a nanoindentation of $\delta = 200$ nm was imposed to the AFM bead. The three dashed lines were shown as a reference. In the first step, due to the action of the stress fibers, the cell experiences a vertical displacement δ_{SF} (with respect to the initial configuration (a)) which is in the nanometer range. At the end of the entire analysis the cell experiences a total vertical displacement $\delta_{TOT} = \delta_{SF} + \delta$.

Figure 4. Scheme of the optimization algorithm implemented to determine the material properties of the ten cell samples investigated.

1
2
3 **Figure 5.** (a) Percent difference between the material properties computed in the presence
4 and in the absence of adhesive structures. (b) Equivalent Young's modulus computed with
5 the proposed optimization algorithm for each sample, compared with the material properties
6 obtained via the Hertz contact theory.
7
8
9
10
11
12
13
14
15

16 **Figure 6.** Comparison of force-indentation curves experimentally retrieved and numerically
17 obtained with the optimization algorithm for the ten cell samples investigated: adhesive cell-
18 substrate structures included in the model.
19
20
21
22
23
24
25

26 **Figure 7.** Comparison of force-indentation curves experimentally retrieved and numerically
27 obtained with the optimization algorithm for the ten cell samples investigated: adhesive cell-
28 substrate structures excluded from the model.
29
30
31
32
33
34
35
36

37 **Figure 8.** Comparison between the force-indentation curves obtained for the same material
38 properties and computed by the optimization algorithm including and excluding the adhesion
39 structures action.
40
41
42
43
44
45
46
47
48
49
50
51
52
53
54
55
56
57
58
59
60